



ELSEVIER

Available online at www.sciencedirect.com

SCIENCE @ DIRECT®

Journal of Marine Systems 49 (2004) 89–103

JOURNAL OF
MARINE
SYSTEMS

www.elsevier.com/locate/jmarsys

Biological heating effect of a band of phytoplankton

Andrew M. Edwards^{a,b,*}, Daniel G. Wright^c, Trevor Platt^a

^aBiological Oceanography Section, Bedford Institute of Oceanography, Dartmouth, Nova Scotia, Canada B2Y 4A2

^bDepartment of Oceanography, Dalhousie University, Halifax, Nova Scotia, Canada B3H 4J1

^cOcean Circulation Section, Bedford Institute of Oceanography, Dartmouth, Nova Scotia, Canada B2Y 4A2

Received 15 October 2002; accepted 3 May 2003

Available online 15 April 2004

Abstract

The presence of phytoplankton in a body of water affects the penetration of irradiance through the water column. This influences the temperature and hence the density distribution of the water. If the phytoplankton concentration varies horizontally, then the consequent density distribution will result in a horizontal pressure gradient. Here we consider a long band (or strip) of high phytoplankton biomass, flanked on either side by clearer water containing little biomass. By means of a simple model, we present calculations of the velocities induced by the pressure gradients to show under what conditions the differential heating effects may become significant. The model's momentum equations assume a steady state, and include effects of Coriolis and vertical eddy viscosity. An analytical solution is obtained, and the induced velocities are shown graphically. Further calculations investigate the potential for the biologically induced vertical velocities to transport nutrients into the surface waters and subsequently influence new primary production. This work demonstrates the capacity for feedbacks from the biological component of the ecosystem to the physical component (and back again).

© 2004 Elsevier B.V. All rights reserved.

Keywords: Modelling; Circulation; Irradiance penetration; Temperature gradient; Feedbacks

1. Introduction

Planktonic organisms are usually considered to be passive participants in the physical dynamics of the ocean. As such, the nature of feedback mechanisms from the biology to the physics is an area of oceanography currently requiring investigation (Robinson et al., 1999). Here we investigate the circula-

tion that could arise in the context of a band (a long strip) of high phytoplankton biomass, flanked by clearer phytoplankton-free water. The surface waters will be heated more within the band than outside it, causing a temperature gradient and hence a density gradient, resulting in a horizontal pressure gradient across the band. We estimate the velocities that could be induced by such a pressure gradient.

Earlier observational and modelling studies have looked at localised temperature increases related to phytoplankton patches. By increasing the attenuation of light in the water column, phytoplankton can cause near-surface waters to become heated more rapidly than if the water were devoid of phytoplankton. Ramp

* Corresponding author. Department of Biology, Dalhousie University, Halifax, NS, Canada B3H 4J1. Tel.: +1-902-494-2146; fax: +1-902-494-3736.

E-mail address: edwardsa@mathstat.dal.ca (A.M. Edwards).

URL: <http://www.chebucto.ns.ca/~english>.

et al. (1991) observed large differences in temperature (up to 4.7 °C) between measurements at depths of 4 cm and 2 m near Point Arena, California. Such temperature differences occurred in areas that were separated on horizontal scales of about 5–10 km by regions where the two temperatures were similar (the situation that one would expect). Concentrations of chlorophyll plus phaeopigments of over 8 mg m⁻³ were measured at a station near where the maximum temperature differences were observed, compared with less than 2 mg m⁻³ at a ‘control’ station that did not show a large temperature difference. With the use of a mixed-layer model, Ramp et al. (1991) concluded that the larger temperature differences were caused by the high concentrations trapping heat very close to the surface (i.e. less than 2 m), coupled with diminished mixing due to low winds.

Ramp et al. (1991) suggested a feedback mechanism whereby a phytoplankton patch starts to form, causing enhanced stratification of the water column and thus accelerating growth by keeping the phytoplankton cells near the surface, resulting in ‘strongly patchy’ chlorophyll distributions. We speculate a related and complementary feedback mechanism, whereby the biologically induced circulation that we calculate could bring nutrient-rich water into the sunlit surface waters, enhancing production.

Kahru et al. (1993) used Advanced Very High Resolution Radiometer (AVHRR) satellite images plus simultaneous ship-board measurements in the Baltic Sea to show that surface accumulation of cyanobacteria (blue-green algae) can cause local increases of sea-surface temperature (SST) of up to 1.5 °C. The patterns of elevated heating associated with cyanobacteria were broken down at night, and occurred on a day of low wind speed (2 m s⁻¹), but not on adjacent days when winds reached 6–9 m s⁻¹.

Such heating effects have been modelled previously, and found to be significant in determining SST in models applied to the Arabian Sea (Sathyendranath et al., 1991) and the eastern North Atlantic Ocean (Simonot et al., 1988), in the timing of the shallowing of the mixed layer (Stramska and Dickey, 1993), and in water column stability (the effect of a deep chlorophyll maximum causing a warm layer of water to develop beneath a colder layer; Lewis et al., 1983).

Considering the Equatorial Pacific Ocean, Lewis et al. (1990) showed that significant solar radiation

penetrates to below the mixed layer, whereas ocean–atmosphere models had assumed that all the radiation was absorbed within the mixed layer. Lewis et al. (1990) noted the sensitivity of SST to chlorophyll concentration, and that optical properties need to be taken into account when modelling the tropical Pacific SST.

Also investigating the Equatorial Pacific, Nakamoto et al. (2001) used an isopycnal ocean general circulation model coupled with a mixed-layer model, to run simulations of circulation both with and without chlorophyll influencing SST. Chlorophyll data were obtained from the Coastal Zone Color Scanner. The simulations with chlorophyll led to shallower mixed-layer depths in the western Equatorial Pacific than the simulation without chlorophyll. But in the eastern Equatorial Pacific the mixed layer became thicker due to changes in the Equatorial Undercurrent. Changes in horizontal velocities reached up to 2–3 cm s⁻¹ (no vertical velocities were given). Nakamoto et al. (2001) concluded that the relatively small thickness and small seasonal excursion of the Equatorial Pacific mixed layer means that this area is particularly vulnerable to any biological heating effect.

Such biological heating may have further consequences. Recently Gildor et al. (2003) suggested that the heating effect of phytoplankton could actually affect intraseasonal variability in the atmosphere. They coupled the nutrient–phytoplankton–zooplankton model of Edwards and Brindley (1999) (which was based on that of Steele and Henderson, 1981) with a simple atmospheric model. Gildor et al. (2003) found that inherent (unforced) oscillations of the biological variables, with a period of about 60 days, could affect SST and induce large-amplitude oscillations in precipitation values (ranging from about 0 to 25 mm day⁻¹). However, the precipitation was low and constant (~3 mm day⁻¹) when biological heating was not considered. Further simulations (with modified parameter values) showed that the precipitation values could oscillate without the biological heating, but that including the biological heating then halved the period of the oscillations to about 60 days. Such a 60-day period is comparable to the typical 40–50 day period exhibited by the so-called tropical intraseasonal oscillation; hence Gildor et al. (2003) speculate a possible biological influence on this atmospheric phenomenon.

On a smaller scale, Trevisan and Bejan (1986) examined how horizontal variations in water turbidity can induce circulation. They considered an idealised stepwise jump in attenuation, broadly similar in concept to our frontal case (Edwards et al., 2001) discussed below. Using a scaling analysis, Trevisan and Bejan (1986) determined the timescales over which diffusion, inertial and viscous effects are important. Coates and Patterson (1993) extended this work by performing experiments in a water-filled Perspex tank, 60 cm long, 20 cm wide and 30 cm high. Radiation entered the water from above, with aluminium foil placed across the left half of the tank such that only the water in the right half was illuminated directly. The consequent heating of the water in the right half established a pressure gradient between the two halves, which created an intrusion of warm near-surface water into the left half. This intrusion was observed within a matter of minutes, in general agreement with the authors' scaling analysis.

Coates and Ferris (1994) repeated these experiments, but included a layer of floating macrophytes underneath the aluminium foil in the non-illuminated half of the tank. The presence of the plants' roots in the water did not prevent the warm intrusion, but did displace it downwards. Coates and Ferris (1994) then estimated the potential for the induced circulation to supply phosphorus-rich water to macrophytes in a small shallow lake, and found that the biological-heating mechanism might make a significant contribution to phosphorus replenishment.

Our approach is to construct a simple model to give estimates of the potential biologically induced velocities. An alternative approach would be to use a more detailed numerical simulation model and include the biologically induced heating effect. However, with such an approach it can be difficult to understand which factors have the most influence upon the results, just as in ecological modelling 'huge simulation models can obscure the action of any of the factors included' (Caswell, 1988). Thus we use a simple model as our interest here is to determine whether or not the biologically induced circulation *could* be significant; we are not trying to simulate a particular set of observations. The understanding gained using the simple model should then aid interpretation of any future study that uses coupled numerical models.

This work extends a previous study (Edwards et al., 2001) in which we considered a phytoplankton profile that might occur in a frontal region, namely a horizontal transition from low to high chlorophyll. We concluded that the resulting velocities could be important, particularly in the vertical direction with regards to transport of nitrate into surface waters. Those results motivate us to extend that work here, by considering a band of phytoplankton and examining the upward transport effect in more detail.

In Section 2, we present the model equations, which we solve analytically (algebraically) to give the biologically induced velocities (mathematical details of the solutions are given in Appendix B). In Section 3 we present the resulting circulation patterns, and in Section 4 we calculate the potential for the biologically induced circulation to enhance the transport of deep nutrient-rich waters to the surface. We assume heat advection to be negligible in our model, an assumption whose validity we examine in detail in Appendix C.

2. Description of model

We consider a band of phytoplankton with maximum chlorophyll biomass in the centre. The biomass diminishes in the x -direction and is assumed to be homogeneous in the y -direction and uniform with depth z (z is positive upwards and has $z=0$ at the position of the water surface in the absence of motion). Such a biomass profile is shown in Fig. 1(a). The attenuation coefficient for irradiance (which includes a chlorophyll-specific component) will thus vary with x , which will result in a spatial distribution of irradiance and thus temperature. This will cause a horizontal variation in the density of the water, and hence result in a horizontal pressure gradient. We use this pressure gradient in the momentum equations to estimate the velocities induced by this biologically induced heating.

We allow for the existence of a physical mechanism that originally helps establish the band of phytoplankton, but here we are concerned only with the additional velocities due to the biological influence, i.e. the velocity perturbations that are due solely to the differential heating effects arising from the chlorophyll gradient. Thus we calculate velocity compo-

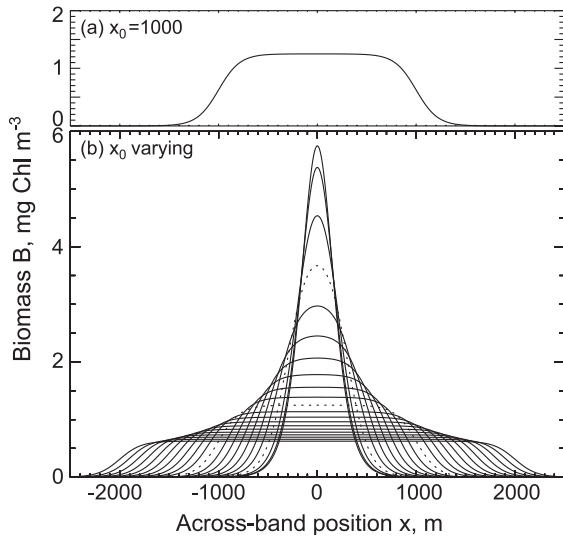


Fig. 1. (a) Biomass profile as given by Eq. (5) using the default parameter values; in particular the centre of the right edge of the band is located at $x_0=1000$ m, the steepness of the edge is $L_0=1000$ m, and the maximum biomass is $1.25 \text{ mg Chl m}^{-3}$ such that total biomass $B_T=2500 \text{ mg Chl m}^{-2}$. (b) The same total biomass as in (a) can take different profiles as x_0 varies in steps of 100 m from 0 (the tallest profile) to 2000 m (the most spread out profile). For illustration, the $x_0=300$ m and $x_0=1000$ m profiles that are used for Fig. 3 are shown as dotted lines.

nents u , v and w in the x , y and z directions, respectively, that are the *perturbations* due solely to the biologically induced density variations.

We first present the momentum equations, followed by the formulation of the biomass profile and calculation of the pressure gradient term. The steady-state momentum equations and the incompressibility equation that we consider are:

$$-fv = -\frac{1}{\rho_0} \frac{\partial p}{\partial x} + A_V \frac{\partial^2 u}{\partial z^2}, \quad (1)$$

$$fu = -\frac{1}{\rho_0} \frac{\partial p}{\partial y} + A_V \frac{\partial^2 v}{\partial z^2}, \quad (2)$$

$$-\rho g = \frac{\partial p}{\partial z}, \quad (3)$$

$$0 = \frac{\partial u}{\partial x} + \frac{\partial v}{\partial y} + \frac{\partial w}{\partial z}, \quad (4)$$

where f is the Coriolis parameter, p is the hydrostatic perturbation pressure resulting from the chlorophyll-induced heating (to be derived), A_V is the constant vertical eddy viscosity, ρ_0 is the typical density of water, ρ is the perturbation density due to the chlorophyll induced heating, and g is the acceleration due to gravity. The Rossby number is small for the conditions considered here, so the advection of momentum can be neglected to give Eqs. (1) and (2). Also, the aspect ratio (vertical/horizontal length scale) is small in all cases considered so that the hydrostatic approximation used in Eq. (3) is valid (Cushman-Roisin, 1994). The boundary conditions are that the surface stress terms $A_V \partial u/\partial z$ and $A_V \partial v/\partial z$ vanish at $z=0$, and there is no induced velocity at great depths (i.e. $u, v, w \rightarrow 0$ as $z \rightarrow -\infty$).

We first prescribe an equation for the horizontal chlorophyll profile, which then leads to equations for the irradiance, temperature and density changes, culminating in an equation for the pressure gradient. These calculations are illustrated using the representative parameter values given in Table 1, which are taken mainly from Edwards et al. (2001), who based such values on the Lewis et al. (1983) study.

Table 1

Definitions of parameters plus the default values used in the calculations, which are mostly as used by Edwards et al. (2001), who mainly took the Scotian Shelf values from Lewis et al. (1983)

Parameter	Symbol	Default value
Specific heat capacity of water	c_p	$4167 \text{ J kg}^{-1} \text{ K}^{-1}$
Coriolis parameter	f	$9.8 \times 10^{-5} \text{ s}^{-1}$
Acceleration due to gravity	g	9.81 m s^{-2}
Attenuation due to chlorophyll	k_c	$0.12 \text{ m}^2 (\text{mg Chl})^{-1}$
Attenuation due to seawater and other substances	k_w	0.072 m^{-1}
Duration of heating	t	43,200 s
Scales width of band	x_0	1000 m
Vertical eddy viscosity	A_V	$0.01 \text{ m}^2 \text{ s}^{-1}$
Total biomass integrated in x-direction	B_T	$2500 \text{ mg Chl m}^{-2}$
Irradiance just below sea surface	I_0	120 W m^{-2}
Distance between 1% and 99% of maximum biomass at edges when band is wide enough	L_0	1000 m
Determines steepness of edges of band	L	$217.4 \text{ m} (=L_0/4.6)$
Thermal expansion coefficient of water	α	$1.668 \times 10^{-4} \text{ K}^{-1}$
Typical density of water	ρ_0	1024 kg m^{-3}

The biomass profile is given by

$$B(x) = \frac{B_T \phi}{2x_0} \left(\frac{1 - \tanh^2 \frac{x}{L}}{1 - \phi^2 \tanh^2 \frac{x}{L}} \right), \quad (5)$$

where

$$\phi = \tanh \frac{x_0}{L}. \quad (6)$$

The motivation for the choice of this formula is given in Appendix A, and our default profile is shown in Fig. 1(a). Essentially, x_0 determines the width of the band, L controls the steepness of the edges and B_T is the ‘total biomass’ within the band. By ‘total biomass’ we mean $B_T = \int_{-\infty}^{\infty} B(x) dx$; recall that biomass is constant in the y and z directions. If x_0 is large enough, as in Fig. 1(a), then the two edges of the band are far enough apart that they can be thought of as two independent frontal cases, for which the biologically induced circulation was determined by Edwards et al. (2001). Here we are concerned with how these circulation patterns interact for bands that are narrower (smaller x_0) and have different steepness at the edges (different L values). The $B_T \phi / (2x_0)$ factor in (5) ensures that as x_0 and L change, the total biomass remains constant (equal to B_T). Fig. 1(b) shows the biomass profile for x_0 varying. The maximum value of biomass becomes higher as x_0 decreases, because the same total amount of biomass (B_T) is concentrated into a narrower band. Thus, these are different possible profiles that a fixed total body of phytoplankton could adopt.

The diffuse vertical attenuation coefficient $k(x)$ (Kirk, 1994) is given by

$$k(x) = k_w + k_c B(x), \quad (7)$$

where k_w is the attenuation due to water in the absence of chlorophyll, and k_c is the specific attenuation coefficient for chlorophyll. Thus, with the Table 1 values, k reaches a maximum of just over 0.22 m^{-1} , which we note is only at the low end of the range of $0.19\text{--}0.47 \text{ m}^{-1}$ measured in the aforementioned study by Ramp et al. (1991). Note that we assume zero background chlorophyll concentration, but this could be relaxed by a simple increase in the value of k_w (e.g.

for a background concentration of $0.1 \text{ mg Chl m}^{-3}$, just increase k_w by $0.1 k_c = 0.012 \text{ m}^{-1}$).

The irradiance $I(x, z)$, W m^{-2} , reaching any location is then given by

$$I(x, z) = I_0 e^{k(x)z}, \quad (8)$$

where I_0 is the irradiance just below the surface (Kirk, 1994). With $I_0 = 120 \text{ W m}^{-2}$ (Table 1), the resulting irradiance penetration through the water column is shown in Fig. 2(a). In the centre the high chlorophyll biomass attenuates the irradiance more strongly near the surface, whereas in the clearer phytoplankton-free water the irradiance can penetrate deeper.

Eqs. (9)–(22) of Edwards et al. (2001), derived for the frontal case, were all expressed in terms of a $k(x)$ of the general form given in Eq. (7), and so those calculations remain valid for the present band case (the explicit formulation of $B(x)$ was not needed). Thus, the temperature increase due to the phytoplankton is again given by Eq. (10) of Edwards et al. (2001), namely

$$T(x, z, t) = \frac{I_0}{\rho_0 c_p} k(x) e^{k(x)z} t, \quad (9)$$

where $T(x, z)$ is the temperature perturbation ($^{\circ}\text{K}$) of the water due to the heating, c_p is the specific heat capacity and t is the duration of heating. Again, we are not taking into account advection and eddy diffusion of temperature, heat losses due to back scattering or heat gains by attenuation of upwelling irradiance, although in Appendix C we do investigate the timescale for which heat advection remains negligible. Fig. 2(b) shows the resulting temperature distribution after a constant irradiance input for 12 h. In the biomass-rich region in the centre, the energy is absorbed near the surface and so the heating is confined to a shallow layer, whereas in the regions with less biomass, the heating is spread deeper into the water column. Near the surface, the water in the centre is warmer than that on the outside, whereas at depth the clearer outside water is warmer (note that the same amount of energy enters the water column at all x locations, unlike in Coates and Pattersons’ (1993) experiments). The depth at which the horizontal temperature gradient reverses direction is

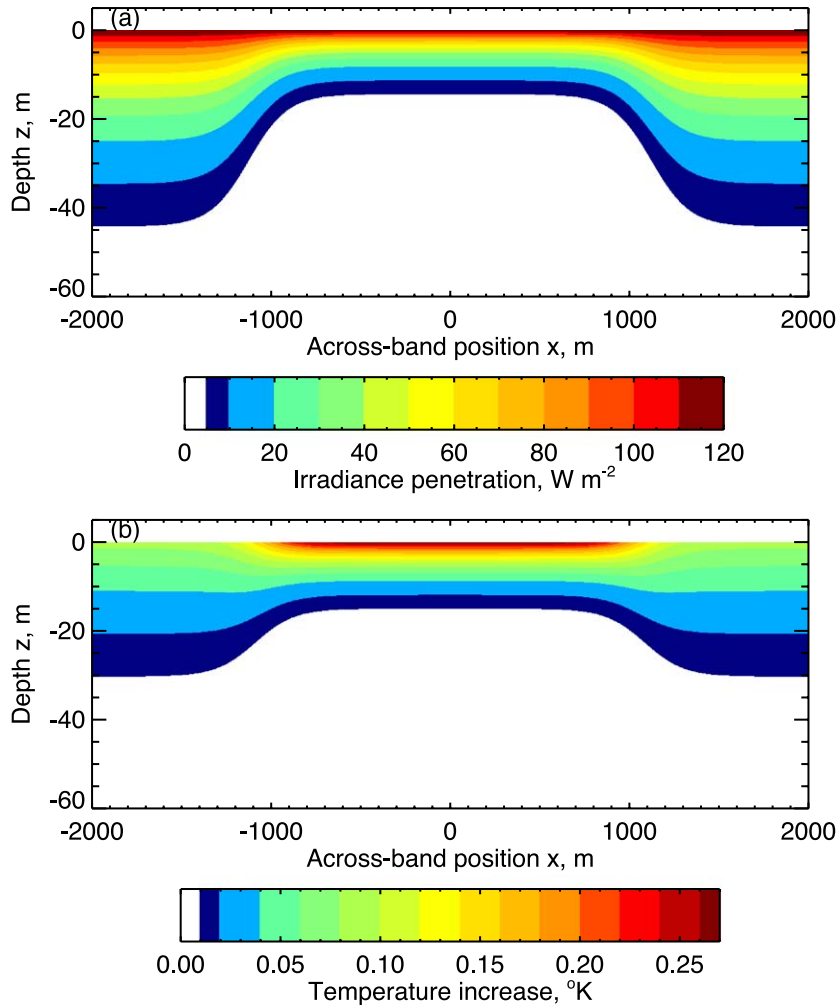


Fig. 2. (a) Irradiance penetration through the water column, resulting from the variation in attenuation coefficient due to the biomass profile shown in Fig. 1(a). (b) Resultant temperature increases after 12 h, given by Eq. (9).

given by the solution to $\partial T/\partial x=0$, which occurs at $x=0$ and at $z=-1/k(x)$, i.e. one optical depth (Kirk, 1994).

The above increases in temperature imply decreases in density, given by the linearised perturbation density

$$\rho = -\rho_0\alpha T, \quad (10)$$

where α is the thermal expansion coefficient (at fixed salinity and pressure, Gill, 1982); see Edwards et al. (2001) for details. The hydrostatic equation, Eq. (3) is now used to give the perturbation pressure $p(x,z,t)$ at any point due to the change in weight of the water

above that point. This results in the perturbation-pressure gradient

$$\frac{\partial p}{\partial x} = \gamma t k'(x) z e^{k(x)z}, \quad (11)$$

where $k'(x)$ is the derivative of $k(x)$. We also have $\partial p/\partial y=0$ because the biomass is homogeneous in the y direction. Since advection and diffusion of heat have been neglected in our idealised calculations, the temperature perturbation increases linearly over time so that t can be considered as a parameter that simply specifies the duration of constant irradiance.

The resulting momentum and incompressibility equations are

$$-fv = -\frac{\gamma t}{\rho_0} k'(x) z e^{k(x)z} + A_v \frac{\partial^2 u}{\partial z^2}, \quad (12)$$

$$f\dot{u} = A_v \frac{\partial^2 v}{\partial z^2}, \quad (13)$$

$$0 = \frac{\partial u}{\partial x} + \frac{\partial v}{\partial y} + \frac{\partial w}{\partial z}. \quad (14)$$

Note that the pressure has been eliminated using Eq. (11). The solutions of Eqs. (12)–(14) for u , v , w and the stream function ψ (which describes the motion in the x – z plane) are obtained analytically, and are given in Appendix B.

3. Resulting circulation patterns

Fig. 3(a) illustrates the biologically induced perturbation velocities when all parameters are set to their default values given in Table 1; in particular, $x_0=1000$ as in Fig. 1(a). The velocity components u , v and w are given by Eqs. (20), (21) and (23) in Appendix B, and are all independent of y . The solutions are the steady-state perturbation velocities, corresponding to a constant irradiance input for 12 h, with all parameters set to the values given in Table 1. The u and w components are represented by the arrows and the streamlines. The *magnitude* of v is given by the coloured shading; two jets occur, the one in the left half of the diagram takes negative v values (out of the page, towards the reader) and the one on the right takes positive values (into the page). There is additionally a small region of weak positive v in the left half (in an area below 40 m), but this is too weak to show up on the colour scale; by symmetry there is a region of negative v in the right half. The streamlines are contours of the stream function (23) given in Appendix B, but note that the contours are not evenly spaced, and are shown simply to help illustrate the circulation. Calculations were performed with Matlab, and IDL was used to produce the diagrams.

The edges of the band are far enough apart that there is very little biomass gradient near $x=0$, see Fig.

1(a), and so the separated left and right frontal regions are essentially equivalent to the frontal situation investigated by Edwards et al. (2001); this is what motivated the functional form of Eq. (5). Thus the circulation pattern that we see in the left region is the same as that shown by Edwards et al. (2001). Because of the symmetry of the biomass profile, the u and v components at any location $x=-x_1$ on the left-hand side will be the negative of the u and v components at $x=x_1$ on the right-hand side. Thus, as x_1 approaches zero the horizontal velocity components must approach zero, with $u=0$ and $v=0$ at $x=0$. This can also be seen from Eqs. (20) and (21) with $k'(0)=0$. The vertical component w , however, has the same sign in each half. Thus, for a narrow enough band the two circulation patterns will combine constructively at $x=0$, strengthening the w component; for the present value of $x_0=1000$, however, this effect is entirely negligible.

A particle in the main clockwise circulation cell on the left-hand side would, in the absence of additional forcing, follow a helical trajectory out of the page; a particle in the right-hand anticlockwise cell would follow a helical trajectory into the page. The strongest u component is $\pm 2.9 \text{ mm s}^{-1}$ at $x=\mp 1010$; $z=-8$ (i.e. $+2.9$ occurred at $x=-1010$ and -2.9 occurred at $x=+1010$); velocity components were calculated at a resolution of 10 m in x and 1 m in z . The maximum downward w component is $w=-0.17 \text{ mm s}^{-1}$, at $x=\pm 920$; $z=-24$, and the strongest upward w component is $w=0.19 \text{ mm s}^{-1}$, at $x=\pm 1150$; $z=-20$. The two jets in the y -direction are strongest at the surface at $x=\pm 1070$, with velocities $v=\pm 1.47 \text{ cm s}^{-1}$. Edwards et al. (2001) unraveled the factors that determine the qualitative nature of the circulation. These maximum speeds are the same as for the default case of Edwards et al. (2001), and so, relative to typical speeds in the ocean, the vertical velocities are again of more potential significance than the horizontal velocities. Furthermore, the vertical velocities are of interest because of the potential extra influx of nutrients into the sunlit surface waters that could be caused by the biologically induced circulation.

This motivates us to consider a narrower band, such that, in particular, the vertical velocities at the centre are enhanced. In Fig. 3(b), we set $x_0=300$, the profile for which is shown as a dotted line in Fig. 1(b). As expected, the more concentrated band

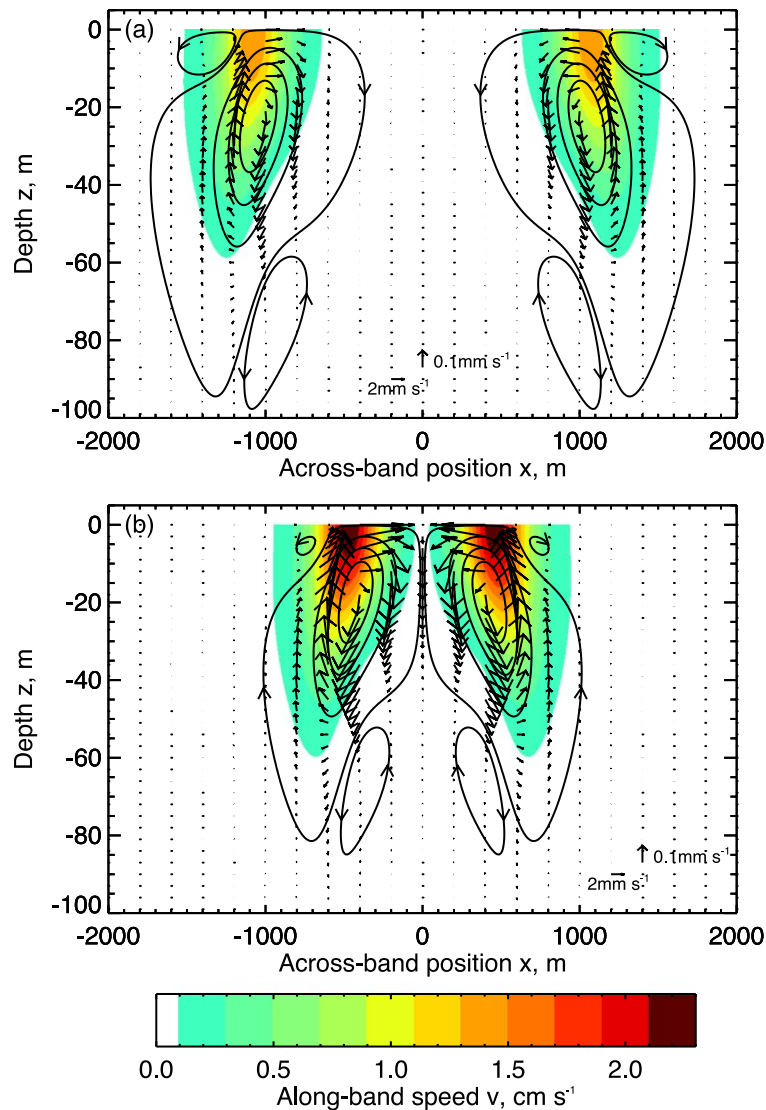


Fig. 3. Biologically induced velocities. The u and w components are represented by arrows and streamlines; arrows indicate the displacement a particle would undergo in approximately 12 h (relative to the x and z scales), and the key shows the actual magnitude of the velocity components. The streamlines are given by constant values of the stream function ψ . The magnitude of the geostrophic along-band velocity v is given by the colour coding—the left-hand jet has negative v values (comes out of the page), and the right-hand jet has positive v values (into the page). (a) All parameters as in Table 1 with $x_0 = 1000$ m, as in Fig. 1(a). (b) With $x_0 = 300$ m, a steeper biomass profile occurs, Fig. 1(b), and the induced velocities become stronger, notably so at $x = 0$.

results in a stronger pressure gradient and hence stronger induced velocities. The strongest u component is $\pm 7.0 \text{ mm s}^{-1}$, at $x = \mp 370$, $z = -3$, the strongest downward w component is -0.32 mm s^{-1} , at $x = \pm 310$, $z = -18$, the strongest upward component is 0.39 mm s^{-1} (approximately 34 m day^{-1}), at

$x = \pm 530$, $z = -16$, and the strongest v is $\pm 2.27 \text{ cm s}^{-1}$, at $x = \pm 460$, $z = 0$.

Note that qualitatively the two circulation patterns in Fig. 3 are the same (three stagnation points for u and w at the surface, the strongest cells in the x – z plane rotate towards the centre and the strongest v is at

the surface); we can predict this analytically, using a similar approach to that in Edwards et al. (2001).

Sensitivity to other parameters was investigated by Edwards et al. (2001) for the frontal case. The default parameters, as used here, were found not to be extreme cases (i.e. they did not necessarily give the strongest velocities). Similar sensitivity calculations would give the same results here.

4. Upward transport calculations

We now calculate the potential for the biologically induced circulation to enhance the transport of deep water to near the surface. Depending on the strength of the transport and the relative nutrient concentrations, such a mechanism could help provide nutrients to the near-surface phytoplankton.

Fig. 4 shows calculations of the total upward transport as x_0 and L_0 are varied. The parameter L_0 is defined as $L_0=4.6L$, and is used because it gives a more intuitive scale than L . When the edges of the band are far enough apart, L_0 gives the distance between the locations that have 1% and 99% of the maximum biomass. Fig. 4 is constructed as follows.

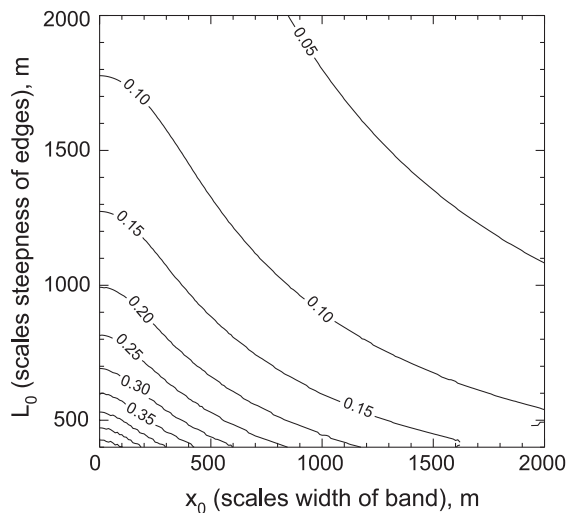


Fig. 4. Contours indicate upward transport, $\text{m}^2 \text{s}^{-1}$, as the shape of the biomass profile varies (lower x_0 means narrower band, lower L_0 means steeper edges of band, with total biomass B_T remaining constant). Calculations are explained in the text. For comparison, the coastal wind-driven Ekman flux for an along-shore 0.1 Pa wind stress is $1 \text{ m}^2 \text{s}^{-1}$.

Fig. 3(a) and (b) each show two main circulation cells in the x - z plane. Along the horizontal line joining the centres of the two cells, the flow is always downwards (w is negative). The integral $\int w \, dx$ along this line gives the total downward transport of water. Since the velocity fields are homogeneous in y , this line is really a horizontal plane between the centres of the two cells, extending forever in y . The downward transport has units of $\text{m}^2 \text{s}^{-1}$, which is interpreted as $\text{m}^3 \text{s}^{-1}$ per metre in the y -direction. Now, since the circulation cells are closed, the downward transport at a particular depth equals the upward transport at that depth (i.e. $\int_{-\infty}^{\infty} w \, dx = 0$). So we compute the integrated w between the centres of the circulations cells, and this gives a value for the downward transport which then equals the upward transport. For the default $x_0=1000 \text{ m}$, $L_0=1000 \text{ m}$ of Fig. 3(a), this equals $0.090 \text{ m}^2 \text{s}^{-1}$. We calculate the transport for each combination of x_0 and L_0 , giving Fig. 4.

We can show analytically (full details are available from the lead author) that for all combinations of x_0 and L_0 shown in Fig. 4 there are two circulation cells at the surface in each half of the x - z plane, and that they have the same directions as those in Fig. 3. This does not guarantee that the dominant circulation cells will remain the ones in Fig. 3 (i.e. clockwise on the left and anti-clockwise on the right), but we have computed further complete circulation diagrams for various combinations of x_0 and L_0 , and indeed the dominant cells always remain qualitatively the same as those in Fig. 3, justifying the transport calculations described in the previous paragraph. Furthermore, the depth of the centres of the circulation cells (given by extrema of the stream function ψ) only varies from 27 to 38 m, where deeper values occur as x_0 increases and the depths are relatively insensitive to L_0 .

In Fig. 4, the computed transport varies from 0.027 to $0.535 \text{ m}^2 \text{s}^{-1}$. The largest values are when x_0 and L_0 are both small, for which the band of phytoplankton is narrow and has steep edges. As x_0 increases the band becomes wider (Fig. 1(b)), and because the total biomass is constant the gradients become smaller and so the transport decreases. In the bottom-right corner of Fig. 4, calculations are not possible because $\phi=\tanh(x_0/L)$ is identically 1 in Matlab double precision arithmetic for $x_0/L > 19$ (i.e. $L_0 < 0.24x_0$); close to these values the extra contour seen in Fig. 4 is similarly a numerical artifact.

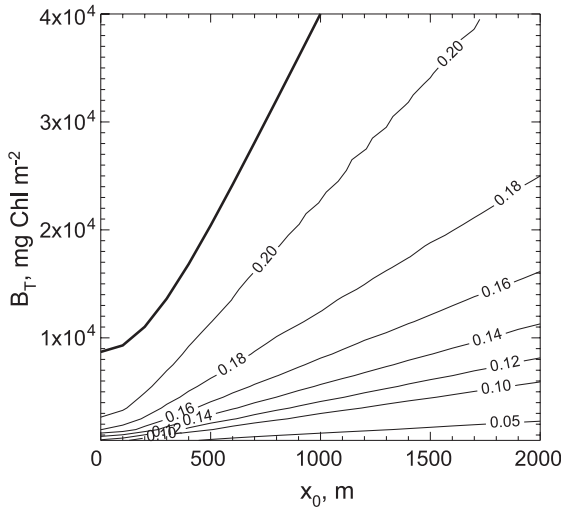


Fig. 5. Upward transport in $\text{m}^2 \text{s}^{-1}$ indicated by the contours, as B_T (total biomass) and x_0 (scales width of band) vary. Note the unevenly spaced contour intervals. No calculations are made to the left of the solid black line because in this area the maximum biomass is greater than 20 mg Chl m^{-3} (the line is thus where $B_T \phi / 2x_0 = 20$).

To give an indication of the relative size of these transport values, we do a simple comparison with a coastal wind-driven Ekman flux. Consider a north–south coastline in the northern hemisphere, with water to the east. Wind blowing to the north will cause surface waters to be transported to the east; these waters will then be replaced by upwelling of deep water. This volume transport is given by $\tau/(\rho_0 f)$, where τ is the wind stress (e.g. Pond and Pickard, 1983). Taking a typical wind stress of 0.1 Pa (about 7.5 m s^{-1}), the upwelling amounts to $1 \text{ m}^2 \text{ s}^{-1}$ (i.e. $1 \text{ m}^3 \text{ s}^{-1}$ per metre in the alongshore direction). Our biologically induced transport calculations are typically an order of magnitude smaller than this (though reaching half the value for the steepest profiles), and so under certain circumstances (e.g. low wind) could be of importance.

Since our idealised scenario produces closed circulation cells, some diffusion mechanism in the deep water would be needed to influx new nitrate to fuel new production. But the circulation could also act to increase regenerated production, by retaining recycled nitrogen (ammonium, dissolved organic nitrogen) within the surface waters. Also, the phytoplankton themselves could be retained nearer the surface,

counteracting any sinking tendency, as demonstrated by Kelley (1997), who showed how convection in ice-covered lakes could be sufficiently strong to retain diatoms in sunlit surface waters and thus enhance primary production.

In Fig. 5 we show how the transport varies with x_0 and total biomass, B_T , keeping L_0 fixed at 1000 m . As the total biomass increases we see that the upward transport also increases. This monotonic behaviour is somewhat expected, but shows that there is no intermediate amount of total biomass that would optimise the transport. A larger total biomass results in a larger temperature gradient and hence stronger induced circulation, but the circulation is confined to narrow regions at the edges of the band, rather than being spread out across the band. One could envisage a situation where such a concentration of the circulation could lead to a decrease in the total transport across the whole band; but this does not seem to occur.

Finally, in Fig. 6 we show how the transport varies with x_0 and L_0 , with the maximum biomass held constant at the default value of $1.25 \text{ mg Chl m}^{-3}$. Note that, in contrast to the previous results, the total biomass B_T is thus varying. Again we find that the transport decreases as x_0 increases from low values, and the transport becomes insensitive to x_0 as x_0 becomes large. Therefore, once the band is wide

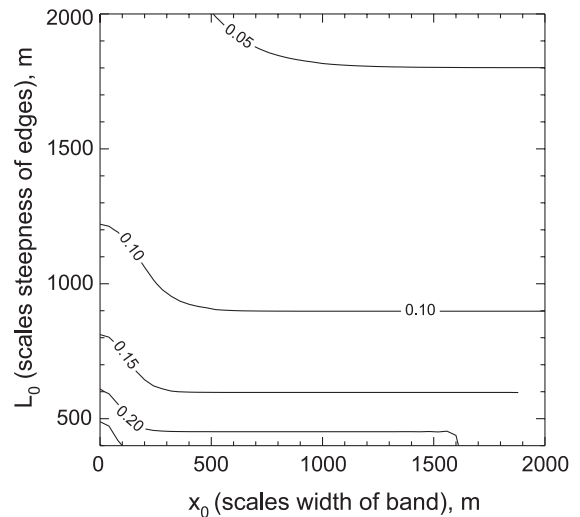


Fig. 6. Upward transport in $\text{m}^2 \text{ s}^{-1}$ as L_0 (steepness of band edges) and x_0 (scales width of band) vary, with the maximum biomass held constant at $1.25 \text{ mg Chl m}^{-3}$ (so B_T now varies).

enough the two main circulation cells do not interact and the transport does not change with x_0 (because the maximum biomass is constant).

5. Discussion

Using a simple model, we have investigated the potential for a biological component of the ocean ecosystem, namely phytoplankton, to influence a physical component, namely the circulation. We have found that the biologically induced heating could produce circulation cells that in turn could have an impact back on the biological production. The enhanced upward transport due to the biological heating could increase new production by upwelling nutrients from deep water, and increase regenerated production by retaining recycled nitrogen. It could also retain negatively buoyant organisms within the euphotic zone (e.g. Kelley, 1997).

Any model must leave some factors out of consideration, just as any experiment must (Caswell, 1988). Running a time-dependent numerical simulation would allow us to drop the steady-state assumption. The analytical steady-state results presented here would prove valuable in interpreting such results; note that our velocity solutions can be considered as quasi-steady-state solutions in the sense that they depend linearly on t , and the time-dependent solutions may then track the steady-state solutions.

Other analytical approaches for coupling advection with biological dynamics have been developed by Robinson (1997), to examine the effects of advection on the dynamics of nutrient, phytoplankton and zooplankton concentrations. Extended work (Robinson, 1999) included light limitation for the phytoplankton. An ambitious project would be to combine these ideas with the work presented here to formulate fully the feedbacks between the biology and the physics.

The effects that we have described here would be difficult to detect in the ocean. It would be hard to distinguish any biologically induced flow from the underlying background physical circulation. The aforementioned experiments of Coates and Patterson (1993) and Coates and Ferris (1994) exhibited a measurable circulation induced by differential heating

across a horizontal gradient, but were performed in a controlled environment and on a much smaller scale than the situation that we describe here. However, large-scale iron fertilisation experiments in the ocean produce isolated patches of phytoplankton, containing high chlorophyll concentrations compared to the background values (similar to our situation). For example, in the Southern Ocean iron release experiment (SOIREE) the original fertilised patch was 7 km in diameter, and over time became stretched into a long ribbon only 4 km wide, with a maximum chlorophyll concentration of 3 mg Chl m⁻³ (Abraham et al., 2000). Our work would be applicable to this and similar situations.

However, the principal utility of our results is to improve the conceptual understanding of feedback processes in the ocean, and to help determine whether biological heating needs to be included in coupled biological–physical models (or even in purely physical models). A factor in such models is the horizontal grid scale. Too coarse a grid scale would not permit the phytoplankton concentration gradient to be steep enough for the biological heating effect to be important. The results presented here suggest the need for more-sophisticated numerical experiments to determine if the effects of biologically induced circulation are important at larger scales than those studied experimentally. If so, parameterisation schemes would need to be developed to include these effects in coarser resolution ocean circulation models.

Acknowledgements

We thank the guest editors Craig Stevens, Joe Ackerman and Catriona Hurd for compiling this special issue and inviting us to contribute to it. We also thank Craig Stevens and the anonymous referees for their suggestions, which have helped to improve the paper. AME acknowledges the financial support of an NSERC Visiting Fellowship in a Canadian Government Laboratory, plus the Department of Fisheries and Oceans Strategic Science Fund. The Department also funded AME's participation at the 2002 ASLO/AGU Ocean Sciences Meeting in Hawaii, which led to consideration of this work for the special issue.

Appendix A. Formulation of biomass profile

We first present the reasoning behind the formulation of the biomass profile Eq. (5). For the frontal case, Edwards et al. (2001) considered the chlorophyll concentration to increase from almost zero to a maximum value B_m along the horizontal x direction, as given by the biomass distribution

$$B(x) = \frac{B_m}{2} \left(1 + \tanh \frac{x}{L} \right), \quad (15)$$

where L determines the steepness of the profile. The profile extends uniformly in the horizontal y direction, and the biomass is uniform with depth. The distance between the locations that have 1% and 99% of the maximum biomass B_m is given by $L_0=4.6L$.

Here we model the chlorophyll concentration $B(x)$ as a symmetric band. Our choice for the specification of $B(x)$ is

$$B(x) = \frac{B_T \phi}{2x_0(1 + \phi)^2} \left(1 + \tanh \frac{x_0 + x}{L} \right) \times \left(1 + \tanh \frac{x_0 - x}{L} \right), \quad (16)$$

where

$$\phi = \tanh \frac{x_0}{L}.$$

Here, B_T is the total biomass (defined shortly), $x_0 > 0$ scales the width of the band, and L determines the steepness of the edges. Note that $0 \leq \phi < 1$. Fig. 1(a) shows such a profile, with $x_0=1000$ m, $L_0=1000$ m and $B_T=2500$ mg Chl m^{-2} . The above formulation is chosen for ease of comparison with the results for a frontal case. In particular, if x_0 is large enough, then the edges of the band will be far enough apart that they can be thought of as two separate ‘frontal’ regions, one at $x=-x_0$ and one at $x=x_0$, symmetric about $x=0$. Therefore, the induced circulation will simply be the same as for a biomass front located at $x=-x_0$, and a mirror image at $x=x_0$; this is the situation in Fig. 3(a). The interesting question is then to discern how these separate circulation patterns combine as x_0 is decreased.

The total biomass B_T is defined as $B_T = \int_{-\infty}^{\infty} B(x) dx$. The extra factors scaling B_T in the first term of Eq.

(16) are such that $\int_{-\infty}^{\infty} B(x) dx$ equals the constant value B_T for all values of x_0 and L . So we have a fixed total quantity of biomass that can spread out or become more concentrated (by varying x_0 and/or L); the area under each of the curves in Fig. 1(b) is the same. The maximum biomass always occurs at $x=0$, and equals $B_T \phi / 2x_0$. In Edwards et al. (2001) our default maximum biomass was 1.25 mg Chl m^{-3} ; setting $B_T \phi / 2x_0 = 1.25$ here, with the aforementioned $x_0=L_0=1000$ m is how we arrived at the value $B_T=2500$ mg Chl m^{-2} .

Eq. (16) can be more concisely written as

$$B(x) = \frac{B_T \phi}{2x_0} \left(\frac{1 - \tanh^2 \frac{x}{L}}{1 - \phi^2 \tanh^2 \frac{x}{L}} \right), \quad (17)$$

which is the formulation that we use.

Note that for $x_0=0$, the first term in Eq. (17) is proportional to $\phi/x_0 = \tanh(x_0/L)/x_0 = 0/0$. But Eq. (17) is not undetermined for $x_0=0$, because using L'Hôpital's Rule (e.g. Thomas, 1968) we find that

$$\lim_{x_0 \rightarrow 0} \frac{\tanh \frac{x_0}{L}}{x_0} = \lim_{x_0 \rightarrow 0} \frac{\frac{1}{L} \operatorname{sech}^2 \frac{x_0}{L}}{1} = \frac{1}{L}, \quad (18)$$

and so for $x_0=0$ we have

$$B(x) = \frac{B_T}{2L} \left(1 - \tanh^2 \frac{x}{L} \right) = \frac{B_T}{2L} \operatorname{sech}^2 \frac{x}{L}. \quad (19)$$

Appendix B. Solutions for velocities

The solutions for the perturbation velocities u , v and w , plus the stream function ψ in the x - z plane, to Eqs. (12)–(14) with boundary conditions $A_V \partial u / \partial z = A_V \partial v / \partial z = 0$ at $z=0$ and $u, v, w \rightarrow 0$ as $z \rightarrow -\infty$, were obtained analytically. These solutions are

$$u = \frac{\gamma t k'(x) \delta_E}{f \rho_0 (k_E(x)^4 + 4)^2} \left\{ e^{z/\delta_E} \left(P_1(x) \cos \frac{z}{\delta_E} + P_2(x) \sin \frac{z}{\delta_E} \right) + 2k_E(x) e^{k(x)z} [(k_E(x)^4 + 4)k(x)z - 2k_E(x)^4 + 8] \right\}, \quad (20)$$

$$v = \frac{\gamma tk'(x)}{f\rho_0(k_E(x)^4 + 4)^2} \left\{ \delta_E e^{z/\delta_E} \left(-P_2(x) \cos \frac{z}{\delta_E} + P_1(x) \sin \frac{z}{\delta_E} \right) + 4e^{k(x)z} [(k_E(x)^4 + 4)z - 4k_E(x)^3 \delta_E] \right\}, \quad (21)$$

$$w = -\frac{2\gamma t A_V}{f^2 \rho_0 (k_E(x)^4 + 4)^3} \left\{ e^{z/\delta_E} \left[2((k_E(x)^4 + 4) \times (3k_E(x)^4 - 4)k''(x) - 4(3k_E(x)^4 - 20)k'(x) \times k'_E(x)k_E(x)^3) \cos \frac{z}{\delta_E} + ((k_E(x)^4 + 4)(k_E(x)^4 - 12)k_E(x)k''(x) - 2(k_E(x)^8 - 48k_E(x)^4 + 48) \times k'(x)k'_E(x))k_E(x) \sin \frac{z}{\delta_E} \right] + 2e^{k(x)z} [(k_E(x)^4 + 4)^2 \times k'(x)^2 k(x)z^2 + ((k_E(x)^4 + 4)k''(x)k(x) - 2(3k_E(x)^4 - 4)k'(x)^2)(k_E(x)^4 + 4)z - (k_E(x)^4 + 4)(3k_E(x)^4 - 4)k''(x) + 4(3k_E(x)^4 - 20)k'(x)k'_E(x)k_E(x)^3] \right\}, \quad (22)$$

$$\psi = \frac{2\gamma t A_V k'(x)}{f^2 \rho_0 (k_E(x)^4 + 4)^2} \left\{ e^{z/\delta_E} \left[2(3k_E(x)^4 - 4) \cos \frac{z}{\delta_E} + (k_E(x)^4 - 12)k_E(x)^2 \sin \frac{z}{\delta_E} \right] + 2e^{k(x)z} [(k_E(x)^4 + 4)k(x)z - 3k_E(x)^4 + 4] \right\}, \quad (23)$$

where

$$P_1(x) = k_E(x)^6 + 6k_E(x)^4 - 12k_E(x)^2 - 8, \quad (24)$$

$$P_2(x) = k_E(x)^6 - 6k_E(x)^4 - 12k_E(x)^2 + 8, \quad (25)$$

$$k_E(x) = k(x)\delta_E, \quad (26)$$

$$\delta_E = \sqrt{\frac{2A_V}{f}}. \quad (27)$$

Edwards et al. (2001) gave full details regarding calculation of the solutions for the frontal case. A

comparable approach was used here. Briefly, Eq. (13) was differentiated twice with respect to z , and $\partial^2 u / \partial z^2$ substituted into Eq. (12) to give an equation in v . The solution (21) for v , in the form of a general solution scaled by e^{z/δ_E} plus a particular solution scaled by $e^{k(x)z}$, was obtained and then used with the boundary conditions to give u . The stream function ψ was obtained from Eq. (14) with $\partial v / \partial y = 0$, and then $w = -\partial \psi / \partial x$ gave w .

Edwards et al. (2001) used the simplification $k''(x)/k'(x) = -(2/L) \tanh(x/L)$, which allowed w to be simplified. However, for the band being considered here, the ratio $k''(x)/k'(x)$ is not so simple and so we leave w in the general form given above (which thus is valid for any suitable function $k(x)$). For the band formulation considered here, the derivatives of $k(x)$ are

$$k'(x) = -\frac{k_c B_T \phi (1 - \phi^2) \operatorname{sech}^2 \frac{x}{L} \tanh \frac{x}{L}}{x_0 L \left(1 - \phi^2 \tanh^2 \frac{x}{L}\right)^2}, \quad (28)$$

$$k''(x) = \frac{k_c B_T \phi (1 - \phi^2) \operatorname{sech}^2 \frac{x}{L}}{x_0 L^2 \left(1 - \phi^2 \tanh^2 \frac{x}{L}\right)^2} \times \left[\phi^2 \tanh^4 \frac{x}{L} + 3(1 - \phi^2) \tanh^2 \frac{x}{L} - 1 \right]. \quad (29)$$

Appendix C. How long is heat advection likely to be negligible?

We have ignored advection in the temperature Eq. (9). However, the circulation patterns shown in Fig. 3 would eventually cause the heated water to be redistributed, influencing the pressure gradient and thus velocities.

We are interested in estimating the effect of the horizontal flow u in the x - z plane, as advection in the y -direction would not change the temperature distribution (because the phytoplankton is assumed homogeneous in the y -direction). The temperature equation including such advection is then

$$\frac{\partial T}{\partial t} + u \frac{\partial T}{\partial x} + w \frac{\partial T}{\partial z} = \frac{1}{\rho_0 c_p} \frac{\partial I}{\partial z}. \quad (30)$$

From the incompressibility Eq. (14) our circulation cells are such that $w/u \sim H/\tilde{L}$, where H and \tilde{L} are, respectively, the vertical and horizontal length scales of the temperature variations. So we can estimate when the advection terms will become important by considering just the horizontal advection term (as the vertical advection will be of the same magnitude).

For our heat advection to be weak, we require

$$\left| u \frac{\partial T}{\partial x} \right| < \chi \frac{1}{\rho_0 c_p} \frac{\partial I}{\partial z}, \quad (31)$$

where $0 < \chi \leq 1$ is a fraction defining the relative magnitudes of the two terms. Setting $\chi=1$ simply means that we demand the advection term to be less than the heat source term, and lower values of χ imply the stricter requirement that the advection term be less than a certain fraction of the source term. For $\chi=1$, our results should still give reasonable order-of-magnitude estimates, but results are more reliable for smaller χ .

The strongest u components occur at $x = \pm x_0$ near the surface for the flows shown in Fig. 3. Also, at $x = \pm x_0$ the horizontal temperature gradient is large near the surface because the biomass gradient is large. So we will calculate order-of-magnitude estimates for the above inequality at $x = -x_0$, for which u is positive.

From Eq. (28) we obtain

$$k'(-x_0) = \frac{k_c B_T \phi^2}{x_0 L (1 + \phi^2)^2}. \quad (32)$$

The function $\phi/(1+\phi^2)$ takes the values 0.500 and 0.496 for $x_0=1000$ and $x_0=300$, respectively, so we take its value to be 0.5, such that

$$k'(-x_0) \sim \frac{k_c B_T}{4x_0 L}. \quad (33)$$

Inserting this and $x = -x_0$ into the solution (20) for u gives an equation of the form

$$u(-x_0) \sim \frac{\Gamma I_0 t}{x_0}, \quad (34)$$

where Γ is a function of x , z and some of the parameters. Here we want to determine an order-of-magnitude estimate for the maximum value of Γ (given the fixed values of most of the parameters). From the aforementioned maximum u value of

$2.9 \times 10^{-3} \text{ m s}^{-1}$ when $x_0=1000 \text{ m}$ we get $\Gamma = 5.8 \times 10^{-7}$. The maximum u of $7.0 \times 10^{-3} \text{ m s}^{-1}$ when $x_0=300 \text{ m}$ gives $\Gamma = 4.1 \times 10^{-7}$. So for our range of interest of x_0 we take $\Gamma \sim 5 \times 10^{-7}$.

To estimate the magnitude of $\partial T/\partial x$ at $x=-x_0$ we have, upon differentiating Eq. (9) with respect to x and using $k(-x_0)=k(x_0)$ for brevity,

$$\frac{\partial T}{\partial x} = \frac{I_0 k_c B_T}{4\rho_0 c_p x_0 L} e^{k(x_0)z} [1 + k(x_0)z] t. \quad (35)$$

Finally, from Eq. (8)

$$\frac{\partial I}{\partial z} = k(x_0) I_0 e^{k(x_0)z}. \quad (36)$$

The inequality in Eq. (31) thus becomes

$$\frac{\Gamma I_0 t}{x_0} \frac{I_0 k_c B_T}{4\rho_0 c_p x_0 L} e^{k(x_0)z} |1 + k(x_0)z| t < \frac{\chi}{\rho_0 c_p} k(x_0) I_0 e^{k(x_0)z}, \quad (37)$$

$$t^2 < \frac{4x_0^2 L k(x_0) \chi}{\Gamma I_0 k_c B_T |1 + k(x_0)z|}. \quad (38)$$

In the near-surface region of interest $z > -2/k(x_0)$, such that $1+k(x_0)z > -1$ and so $|1+k(x_0)z| < 1$. Therefore, a bound for t^2 that is even stricter than that in Eq. (38) is

$$t^2 < \frac{4x_0^2 L k(x_0) \chi}{\Gamma I_0 k_c B_T}; \quad (39)$$

i.e. if Eq. (39) is violated then Eq. (38) may still hold. Then using $k(x_0) = k_w + k_c B_T / (4x_0)$ we have

$$t^2 < \frac{L x_0 \chi}{\Gamma I_0} \left(1 + \frac{4k_w x_0}{k_c B_T} \right). \quad (40)$$

Putting in values (except x_0 and χ) and defining $t_h = t/3600$ to be the time in hours, our limit is

$$t_h < 0.53 \sqrt{x_0 \chi \left(1 + \frac{x_0}{1042} \right)}. \quad (41)$$

So the timescale t_h , for which advection is less than a fraction χ of the heating term, increases with

the square root of x_0 until the $x_0/1042$ factor becomes important. Setting $\chi=1$, for $x_0=1000$ this bound is approximately 23 h and for $x_0=300$ it is approximately 10 h. Thus, the maximum magnitude of the temperature advection term would be of the same order as the temperature source term after about 23 and 10 h, respectively. With the stricter value of $\chi=1/4$, the times are 12 and 5 h for $x_0=1000$ and 300, respectively.

Thus for our original value of $x_0=1000$, the assumption of ignoring temperature advection is valid for the 12 h time-frame considered. Whereas for the more compact band with $x_0=300$, the advection will become important in less than 12 h, because the steeper chlorophyll gradient leads to a steeper horizontal temperature gradient and higher induced velocities. Note, however, that our bound in Eq. (41) is overly strict due to the simplification between Eqs. (38) and (39).

References

- Abraham, E.R., Law, C.S., Boyd, P.W., Lavender, S.J., Maldonado, M.T., Bowie, A.R., 2000. Importance of stirring in the development of an iron-fertilized phytoplankton bloom. *Nature* 407, 727–730.
- Caswell, H., 1988. Theory and models in ecology: a different perspective. *Ecol. Model.* 43, 33–44.
- Coates, M., Ferris, J., 1994. The radiatively driven natural convection beneath a floating plant layer. *Limnol. Oceanogr.* 39, 1186–1194.
- Coates, M.J., Patterson, J.C., 1993. Unsteady natural convection in a cavity with nonuniform absorption of radiation. *J. Fluid Mech.* 256, 133–161.
- Cushman-Roisin, B., 1994. Introduction to Geophysical Fluid Dynamics, Prentice-Hall, Upper Saddle River, NJ.
- Edwards, A.M., Brindley, J., 1999. Zooplankton mortality and the dynamical behaviour of plankton population models. *Bull. Math. Biol.* 61, 303–339.
- Edwards, A.M., Platt, T., Wright, D.G., 2001. Biologically induced circulation at fronts. *J. Geophys. Res.* 106, 7081–7095.
- Gildor, H., Sobel, A.H., Cane, M.A., Sambrotto, R.N., 2003. A role for ocean biota in tropical intraseasonal atmospheric variability. *Geophys. Res. Lett.* 30 (9), 1460 (doi:10.1029/2002GL016759).
- Gill, A.E., 1982. Atmosphere–Ocean Dynamics Academic Press, New York.
- Kahru, M., Leppänen, J.-M., Rud, O., 1993. Cyanobacterial blooms cause heating of the sea surface. *Mar. Ecol., Prog. Ser.* 101, 1–7.
- Kelley, D.E., 1997. Convection in ice-covered lakes: effects on algal suspension. *J. Plankton Res.* 19, 1859–1880.
- Kirk, J.T.O., 1994. Light and Photosynthesis in Aquatic Ecosystems, Second edition, Cambridge Univ. Press, Cambridge.
- Lewis, M.R., Cullen, J.J., Platt, T., 1983. Phytoplankton and thermal structure in the upper ocean: consequences of nonuniformity in chlorophyll profile. *J. Geophys. Res.* 88, 2565–2570.
- Lewis, M.R., Carr, M., Feldman, G.C., Esaias, W., McClain, C., 1990. Influence of penetrating solar radiation on the heat budget of the equatorial Pacific Ocean. *Nature* 347, 543–545.
- Nakamoto, S., Prasanna Kumar, S., Oberhuber, J.M., Ishizaka, J., Muneyama, K., Frouin, R., 2001. Response of the equatorial Pacific to chlorophyll pigment in a mixed layer isopycnal ocean general circulation model. *Geophys. Res. Lett.* 28, 2021–2024.
- Pond, S., Pickard, G.L., 1983. Introductory Dynamical Oceanography, Second edition, Pergamon, Oxford.
- Ramp, S.R., Garwood, R.W., Davis, C.O., Snow, R.L., 1991. Surface heating and patchiness in the coastal ocean off central California during a wind relaxation event. *J. Geophys. Res.* 96, 14947–14957.
- Robinson, A.R., 1997. On the theory of advective effects on biological dynamics in the sea. *Proc. R. Soc. Lond., A* 453, 2295–2324.
- Robinson, A.R., 1999. On the theory of advective effects on biological dynamics in the sea: II. Localization, light limitation, and nutrient saturation. *Proc. R. Soc. Lond., A* 455, 1813–1828.
- Robinson, A.R., McCarthy, J.J., Rothschild, B.J., 1999. Interdisciplinary ocean science is evolving and a systems approach is essential. *J. Mar. Syst.* 22, 231–239.
- Sathyendranath, S., Gouveia, A.D., Shetye, S.R., Ravindran, P., Platt, T., 1991. Biological control of surface temperature in the Arabian Sea. *Nature* 349, 54–56.
- Simonot, J.-Y., Dollinger, E., Le Treut, H., 1988. Thermodynamic–biological–optical coupling in the oceanic mixed layer. *J. Geophys. Res.* 93, 8193–8202.
- Steele, J.H., Henderson, E.W., 1981. A simple plankton model. *Am. Nat.* 117, 676–691.
- Stramska, M., Dickey, T.D., 1993. Phytoplankton bloom and the vertical thermal structure of the upper ocean. *J. Mar. Res.* 51, 819–842.
- Thomas, G.B., 1968. Calculus and Analytic Geometry, Fourth edition, Addison-Wesley Publishing, Reading, MA.
- Trevisan, O.V., Bejan, A., 1986. Convection driven by the nonuniform absorption of thermal radiation at the free surface of a stagnant pool. *Numer. Heat Transf.* 10, 483–506.